



Methods in eye research

Photoacoustic tomography imaging and estimation of oxygen saturation of hemoglobin in ocular tissue of rabbits



Stella N. Hennen^{a, b, *, 1}, Wenxin Xing^{c, d, 1}, Ying-Bo Shui^b, Yong Zhou^d, Jennifer Kalishman^e, Lisa B. Andrews-Kaminsky^e, Michael A. Kass^b, David C. Beebe^b, Konstantin I. Maslov^{c, d}, Lihong V. Wang^{c, d, **}

^a Solo Private Practice, Minneapolis, MN, USA

^b Department of Ophthalmology and Visual Sciences, School of Medicine, Washington University in St. Louis, St. Louis, MO, USA

^c Department of Electrical and Systems Engineering, Washington University in St. Louis, St. Louis, MO, USA

^d Optical Imaging Laboratory, Department of Biomedical Engineering, School of Engineering and Applied Science, Washington University in St. Louis, St. Louis, MO, USA

^e Division of Comparative Medicine, School of Medicine, Washington University School of Medicine in St. Louis, St. Louis, MO, USA

ARTICLE INFO

Article history:

Received 3 December 2014

Received in revised form

27 May 2015

Accepted in revised form 30 May 2015

Available online 3 June 2015

Keywords:

Oxygen

Saturation

Photoacoustic tomography

Rabbit

ABSTRACT

This study evaluated *in vivo* imaging capabilities and safety of qualitative monitoring of oxygen saturation of hemoglobin (sO_2) of rabbit ciliary body tissues obtained with acoustic resolution (AR) photoacoustic tomography (PAT). AR PAT was used to collect trans-scleral images from ciliary body vasculature of seven New Zealand White rabbits. The PAT sO_2 measurements were obtained under the following conditions: when systemic sO_2 as measured by pulse oximetry was between 100% and 99% (level 1); systemic sO_2 as measured by pulse oximetry was between 98% and 90% (level 2); and systemic sO_2 as measured by pulse oximetry was less than 90% (level 3). Following imaging, histological analysis of ocular tissue was conducted to evaluate for possible structural damage caused by the AR PAT imaging.

AR PAT was able to resolve anatomical structures of the anterior segment of the eye, viewed through the cornea or anterior sclera. Histological studies revealed no ocular damage. On average, sO_2 values (%) obtained with AR PAT were lower than sO_2 values obtained with pulse oximetry (all $p < 0.001$): 86.28 ± 4.16 versus 99.25 ± 0.28 , 84.09 ± 1.81 vs. 95.3 ± 2.6 , and 64.49 ± 7.27 vs. 71.15 ± 10.21 for levels 1, 2 and 3 respectively. AR PAT imaging modality is capable of qualitative monitoring for deep tissue sO_2 in rabbits. Further studies are needed to validate and modify the AR PAT modality specifically for use in human eyes. Having a safe, non-invasive method of *in vivo* imaging of sO_2 in the anterior segment is important to studies evaluating the role of oxidative damage, hypoxia and ischemia in pathogenesis of ocular diseases.

Published by Elsevier Ltd.

1. Introduction

Numerous studies have identified oxidative damage as an important event in the pathogenesis of ocular diseases such as

macular degeneration (Kinnunen et al., 2012), cataract (Varma et al., 2011), and glaucoma (Abu-Amero et al., 2006; Alvarado et al., 1981; Chang, 2006; Chen and Kadlubar, 2003; Ferreira et al., 2004; Gabelt and Kaufman, 2005; Holekamp et al., 2005; Izzotti et al., 2003; Izotti et al., 2006; Izzotti et al., 2009; Kong et al., 2009; Liton et al., 2009; Sacca et al., 2005, 2007; Sacca and Izzotti, 2008; Shui et al., 2006; Siegfried et al., 2010; Tomarev, 2001; Wang et al., 2001; Zhou and Yue, 1999). Two important hemodynamic parameters of oxygen metabolism include oxygen partial pressure (pO_2) and oxygen saturation of hemoglobin (sO_2). pO_2 represents the amount of free oxygen concentration available to cells. sO_2 represents the amount of oxygen carried by hemoglobin. The relationship between pO_2 and sO_2 , referred as the

* Corresponding author. Eyecare MPLS PLLC, 3033 Excelsior Blvd, Suite 205, Minneapolis, MN 55416, USA.

** Corresponding author. Optical Imaging Laboratory, Department of Biomedical Engineering, School of Engineering and Applied Science, Washington University in St. Louis, Campus Box 1097, One Brookings Drive, St. Louis, MO 63130, USA.

E-mail addresses: stella0213@gmail.com (S.N. Hennen), lhwang@seas.wustl.edu (L.V. Wang).

¹ Stella Hennen and Wenxin Xing contributed equally to this work.

hemoglobin oxygen dissociation curve, describes how blood carries and releases oxygen for tissue metabolism under physiological and pathological conditions (Wang, 2008). We demonstrated that redistribution of oxygen in the anterior segment following vitrectomy and cataract surgery leads to increased pO_2 in the posterior chamber (PC) and anterior chamber (AC) angle, which is potentially damaging to the trabecular meshwork cells. Hence, measuring pO_2 in the PC and AC angle may identify eyes at risk for development of glaucoma (Holekamp et al., 2005; Shui et al., 2006; Siegfried et al., 2010).

Since sO_2 and pO_2 are related, it is reasonable to postulate that sO_2 , similar to pO_2 may play an important role in early diagnosis of glaucoma. A novel powerful optical imaging modality called photoacoustic tomography (PAT) is capable of non-invasive *in vivo* imaging of intra-vascular total hemoglobin concentration (HbT) and sO_2 (de la Zerdá et al., 2010; Hoelen et al., 1998; Hu et al., 2010; Jiao et al., 2009, 2010; Jiang et al., 2010; Kong et al., 2009a, 2009b; Maslov et al., 2008; Rao et al., 2010; Rosencwaig, 1982; Silverman et al., 2010; Song et al., 2013; Wang et al., 2003, 2006; Wang and Wu, 2007; Wang, 2008; Wang et al., 2011; Xie et al., 2009; Xing et al., 2013; Yao and Wang, 2011; Zhang et al., 2006, 2007, 2010, 2010).

In addition to measuring sO_2 , PAT can also provide structural imaging at a higher resolution than coherence tomography (OCT) and deeper penetration than ultrasound (US). Because OCT relies on ballistic photon detection, the penetration depth is limited to ~1 mm in biological tissue due to high optical scattering. On the contrary, US has very small scattering in the soft tissue, and thus it has deeper tissue penetration but lower resolution than OCT (Kong et al., 2009a; Yao and Wang, 2011). PAT overcomes limitations of OCT and US. Thus, deep embedded structures (such as ocular tissue in the rabbit eye) can be successfully detected by PAT.

PAT obtains *in vivo* cross-sectional three-dimensional high-resolution structural, functional, and molecular images by utilizing the photoacoustic effect discovered by Alexander G. Bell in 1880 (Yao and Wang, 2011). When tissue is irradiated by a laser beam, locally absorbed light is converted into heat. The heat causes thermoelastic expansion of the tissue and rise in pressure. The pressure rise propagates in the tissue as an ultrasonic wave, also known as a photoacoustic wave. The photoacoustic wave is detected by ultrasonic transducers that convert it into electrical signals. The electric signals are amplified, digitalized, and analyzed by a computer to form images (Wang, 2008). Because the amplitude of the photoacoustic wave is proportional to the energy absorbed by the object, multiple optical wavelengths can be used in PAT to provide spectral information of optical absorption. In addition, because oxygenated hemoglobin (HbO₂) and deoxygenated hemoglobin (Hb) have different absorption spectrum, sO_2 can be successfully measured by PAT with high accuracy and high spatial resolution (Wang, 2008). PAT can operate in two modes: optical resolution and acoustic resolution. Optical resolution PAT is useful for imaging of blood vessels near the surface and acoustic resolution (AR) PAT is more effective in imaging at greater depth.

The goal of this study was to evaluate imaging capabilities and safety of *in vivo* qualitative monitoring of oxygen saturation of hemoglobin (sO_2) of rabbit ciliary body tissues obtained with AR PAT technique.

2. Methods

All experimental animal procedures were approved by the Institutional Animal Care and Use Committee of Washington University in St. Louis and adhered to the EU Directive 2010/63/EU for animal experiments. This pilot study involved 7 adult New Zealand White rabbits. The rabbits were anesthetized with a combination of

ketamine:xylazine (15 mg/kg:2 mg/kg) intramuscularly, intubated, ventilated, and maintained on isoflurane gas throughout the imaging procedure. Using AR PAT we imaged the same area of the anterior segment of one eye of each rabbit three times. The signals from ciliary body blood vessels were analyzed to calculate the averaged absolute sO_2 . Volume imaged was $2.6 \times 10^5 \text{ um}^3$.

To confirm the ability of the AR PAT imaging to respond to changes in ocular HbT and sO_2 among various conditions, the PAT sO_2 measurements were obtained under following the conditions: systemic sO_2 as measured by pulse oximetry between 100% and 99% (level 1); systemic sO_2 as measured by pulse oximetry between 98% and 90% (level 2); and systemic sO_2 as measured by pulse oximetry less than 90% (level 3). We intentionally modified the percentage of oxygen in the inspired to achieve these different sO_2 levels. In this study we wished to demonstrate a qualitative ability of AR PAT to monitor increases and decreases in tissue saturation thus high levels of oxygen in the inspired gas was used. Systemic sO_2 was monitored by pulse oximetry. A clamp-type pickup was used on the animal's back paw. In order to determine if tissue damage was produced by the laser exposure we conducted histological studies. We included 4 rabbits with various life endpoints after AR PAT imaging experiments: 30 min (one rabbit); one day (one rabbit); and one week (two rabbits). The cornea, iris, trabecular meshwork, lens, choroid, vitreous, and retina of all animals were evaluated histologically using light microscopy and hematoxylin and eosin staining for any possible structural damage caused by the AR PAT imaging due to laser light. The contra-lateral non-imaged eyes were used as controls.

2.1. AR PAT modality

Schematics of AR PAT used in the experiment are shown in Fig. 1. A tunable dye laser (Sirah) pumped by a 523-nm-wavelength Nd:YLF laser (EdgeWave) was used for sound excitation. Rhodamine 6G was chosen as the dye to provide tunable wavelength from 560 nm to 580 nm with a pulse width around 5 ns. The laser beam was delivered to the scanning stage via 600 μm core diameter multimode optical fiber (Thorlabs). Emerging out of the tip, the light was ring shaped by a conical lens, passed around a 1/4" diameter, 8 mm focal length, 20 MHz ultrasonic transducer (Panametrics Inc., model V212-BB-RM), and weakly focused into the sample by an optical condenser. The incident fluence on the tissue surface was estimated to be about 5 mJ/cm^2 , which was less than the safety limit set by the American National Standard Institute (ANSI) (20 mJ/cm^2). A focused ultrasonic transducer was immersed in a water tank. The bottom of the water tank was a layer of 25 μm LDPE membrane closely attached to the sample and acoustically coupled by ultrasonic gel. During raster scanning along the sample surface the electrical signal from the ultrasonic transducer was collected, amplified, digitized, and transferred to computer to form 3D images. A part of the laser pulse was directed to the photodiode used to account for the energy variations of the laser pulses.

Taking into account that amplitude of the photoacoustic signal is proportional to the local optical absorption coefficient, the relative oxy- and deoxy-hemoglobin concentrations can be estimated by solving the following equations:

$$\mu_a(\lambda_1) = 2.303 \times (\epsilon_{ox}(\lambda_1)C_{ox} + \epsilon_{de}(\lambda_1)C_{de})$$

$$\mu_a(\lambda_2) = 2.303 \times (\epsilon_{ox}(\lambda_2)C_{ox} + \epsilon_{de}(\lambda_2)C_{de})$$

where $\mu_a(\lambda_1)$ and $\mu_a(\lambda_2)$ are absorption coefficients of the blood at two wavelengths; ϵ and C are the molar extinction coefficients and concentrations, respectively; ox and de refer to oxy- and

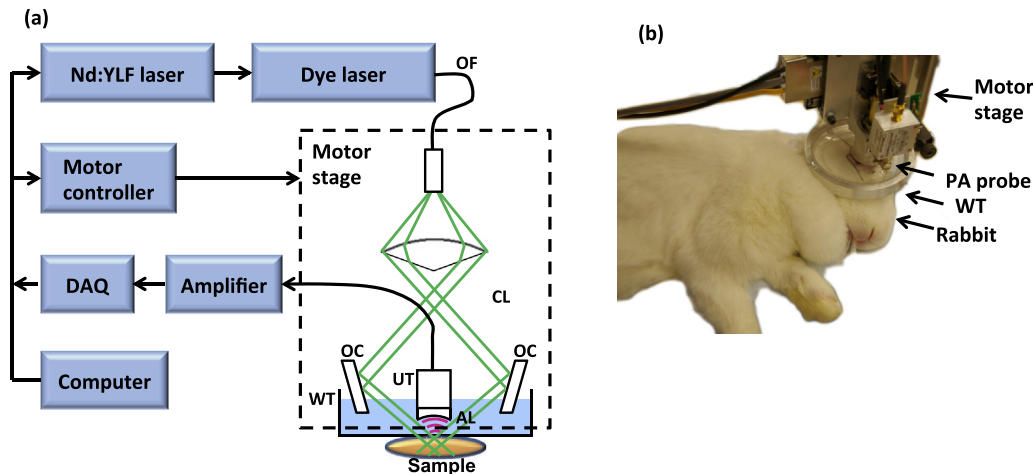


Fig. 1. (a) Schematic of the acoustic-resolution (AR) – photoacoustic microscopy (PAM) system. AL = acoustic lens; CL = conical lens; OF = optical fiber; OC = optical condenser; UT = ultrasound transducer; WT = water tank. (b) Photograph of the system in place.

deoxyhemoglobin, respectively. The oxygen saturation of hemoglobin can be obtained as following:

$$sO_2 = \frac{C_{ox}}{C_{ox} + C_{de}} \times 100$$

In each imaging procedure, two wavelengths, 578 nm or 563 nm, were chosen to differentiate Hb and HbO₂. Although wavelength dependent scattering could cause errors in calculating the sO₂ values, wavelengths we used were very close. Therefore the difference in path length was negligible. Thus, there was no need for a calibration factor (Zhang et al., 2006). Wavelengths were switched between b-scans (cross-sectional image) and the acquisition rate of each b-scan was 2 Hz. The system spatial resolutions, determined by the ultrasonic transducer, were about 70 μm in the lateral direction and 54 μm in the axial direction, both smaller than the dimension of ciliary body. To ensure that we detected signal solely from the ciliary body we only chose only that area for analysis. Since we selected AR PAT to work at greater depth, this lead to loss of resolution of the individual vessels. Therefore, instead of measuring sO₂ from a single blood capillary, we calculated an average value from all blood vessels in the measured area based on the PAT detection.

3. Results

We were able to successfully resolve the anatomy of the anterior segment of the rabbit eye including iris, ciliary body, and anterior choroid (Fig. 2). Histological evaluation using light microscopy and hematoxylin and eosin stains demonstrated no laser damage to the ocular tissue up to one week following AR PAT imaging (Fig. 3). In the non-survival experiments, on average, sO₂ values obtained with AR PAT were lower than sO₂ values (%) obtained with pulse oximetry (all p < 0.001): 86.28 ± 4.16 versus 99.25 ± 0.28, 84.09 ± 1.81 vs. 95.3 ± 2.6, and 64.49 ± 7.27 vs. 71.15 ± 10.21 in the settings of: oxygen percentage in breathing gas between 99% and 100% (level 1); oxygen percentage in breathing gas between 90% and 98% (level 2); and oxygen percentage in breathing gas less than 90% (level 3) respectively (Fig. 4).

4. Discussion

The current study demonstrated that AR PAT imaging can

successfully, non-invasively, and safely resolve the anatomy of the anterior segment of the eye. The laser energy was carefully controlled and focused towards the sclera in order to avoid direct exposure of the lens and retina. Further protection such as application of a contact lens covering the iris is possible.

We also demonstrated that AR PAT can qualitatively monitor the sO₂ change in blood vessels of the ciliary body. We found that sO₂ qualitative monitoring obtained with AR PAT yielded values that were significantly lower than sO₂ measurements obtained with pulse oximetry. These results would be expected since systemic pulse oximetry only measures arterial sO₂ whereas AR PAT calculates an average value from both arterial vessels (that have high oxyhemoglobin concentration hence high sO₂) and venous vessels, which contain both oxyhemoglobin and deoxyhemoglobin resulting in lower overall sO₂. Further, due to imaging of deep tissue AR PAT couldn't resolve individual vessels. Instead it qualitatively monitored an averaged sO₂ of the entire vascular bed. A reliable qualitative monitoring with ranges that correlate with hyperoxia, normoxia and hypoxia would be especially valuable for early detection and monitoring of the conditions that affect tissue saturation. Our study showed that AR PAT is a promising method for qualitative monitoring of the deep tissue, which also might be useful for monitoring oxidative damage studies in eyes.

Our technique should work similarly in pigmented animals or humans. Because our AR PAT system has high spatial resolutions, the pigment would not interfere with the sO₂ imaging of deeply embedded ocular vasculatures. However, we would have to consider changing the imaging wavelengths to avoid strong attenuation due to the pigments. For an example, for a melanin-rich sample, a longer wavelength would be used, because melanin has smaller absorption at longer wavelength.

Previously we performed PAT imaging of rat brains *in vivo* under normoxic, hyperoxic, and hypoxic conditions. We successfully demonstrated simultaneous assessment of the blood volume, HbT, and sO₂ of the cerebral vasculature (Wang et al., 2006). We recently developed a dual-modality microscope integrating PAT and fluorescence confocal microscopy (FCM) that can simultaneously image sO₂ and pO₂ *in vivo* in a single blood vessel (Wang et al., 2011). Other investigators demonstrated the ability of PAT to successfully image blood distribution in live rats and rabbits (de al Zerdá et al., 2010; Jiang et al., 2010; Xie et al., 2009; Zhang et al., 2010a). We previously demonstrated the feasibility of PAT imaging of microvasculature of the ear, brain, and skin (Maslov et al., 2008; Rao et al.,

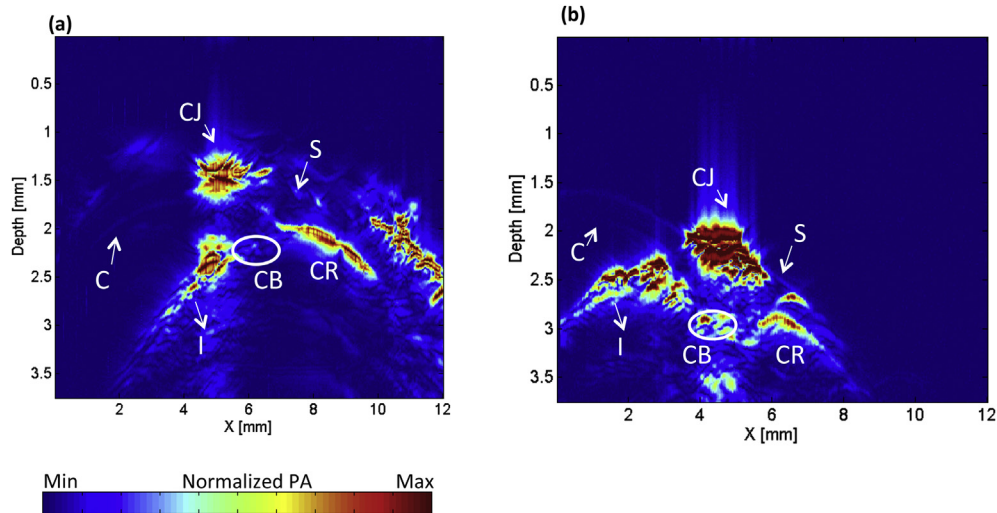


Fig. 2. Photoacoustic image of rabbit eye. (a) and (b) Images of eye from a different angle. C = Cornea; CB = ciliary body; CJ = Conjunctiva; CR = Choroid; I = Iris; S = Sclera.

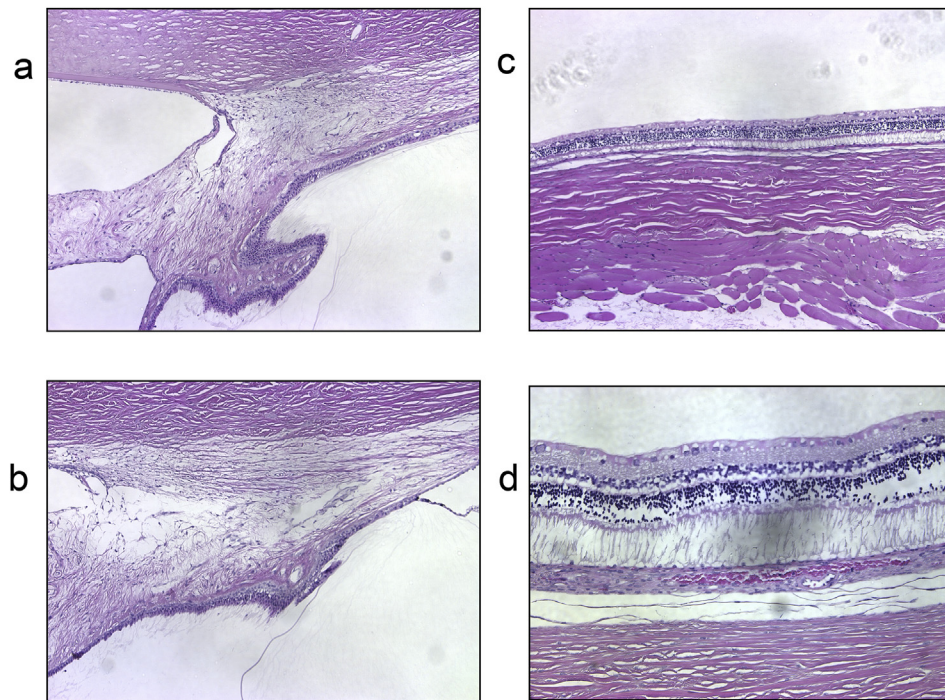


Fig. 3. Histological evaluation using light microscopy and hematoxylin and eosin stains: (a). Ciliary body imaged with photoacoustic tomography (PAT); (b). Control ciliary body; (c). Retina imaged with PAT; (d). Control retina.

2010; Zhang et al., 2006). PAT is also capable of evaluating the metabolic rate of oxygen (MRO_2). Although other modalities can also evaluate MRO_2 , they have limitations. Magnetic resonance imaging only detects temporal changes in hemoglobin concentration. Positron emission tomography requires exogenous radioactive tracers to image MRO_2 (Yee et al., 2006). Diffuse optical tomography has low spatial resolution (Culver et al., 2003). In contrast, PAT has a potential to become a single modality to image *in vivo* MRO_2 , blood vessels and other structures of interest, and estimate blood flow without exogenous contrast (Wang, 2008). Currently, MRO_2 measurements can't be obtained in the AR PAT system because of its limited detection of flow rate. However a new cross-correlation based method which measures blood-flow velocity by using

photoacoustic microscopy may achieve *in vivo* deep flow monitoring by increasing the detection time and thus providing a potential solution for MRO_2 measurement (Liang et al., 2013; Zhou et al., 2013).

The eye has an abundance of endogenous contrasts such as hemoglobin, melanin, and vascular tissue. All can be readily quantified and imaged by the PAT technique (de la Zerde et al., 2010; Hu et al., 2010; Jiao et al., 2010; Jiang et al., 2010; Rao et al., 2010; Silverman et al., 2010; Song et al., 2013; Xie et al., 2009; Zhang et al., 2010a, 2010b). PAT imaging of *ex vivo* sectioned pig eyes demonstrates that using focused laser beam short pulse irradiation with a ring ultrasonic transducer provides sharper ocular images than an unfocused laser (Kong et al., 2009a). Laser with

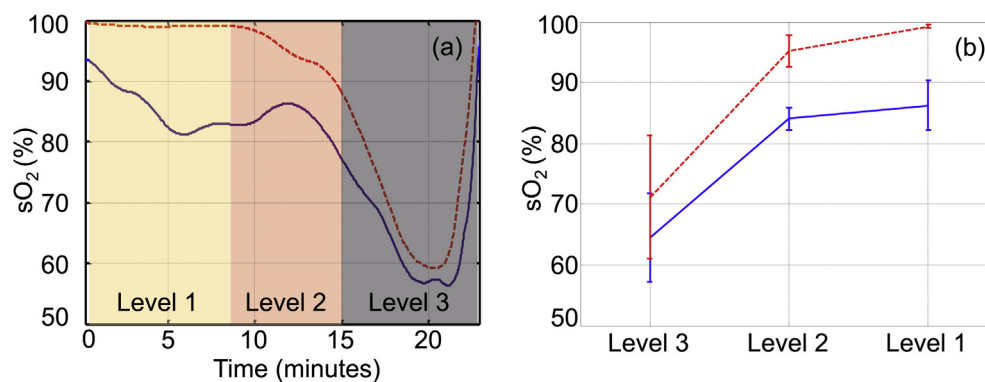


Fig. 4. Oxygen saturation (sO_2) qualitative monitoring of rabbit ciliary body vasculature obtained by photoacoustic tomography (PAT) under the following conditions: systemic sO_2 as measured by pulse oximetry between 100% and 99% (level 1); systemic sO_2 as measured by pulse oximetry between 98% and 90% (level 2); and systemic sO_2 as measured by pulse oximetry less than 90% (level 3). Red dashed line: systemic sO_2 measured by pulse oximeter. Blue solid line: sO_2 qualitative monitoring by PAT. (a) Time trace of sO_2 qualitative monitoring. (b) sO_2 mean value and corresponding standard deviations of sO_2 in those conditions. Systemic pulse oximetry values are plotted on axis Y.

1064 nm near infra-red wavelength provides better penetration but lower sensitivity than laser with 532 nm green wavelength, which provides sharper images of cornea, lens surface, iris, ciliary body, and zonules (Silverman et al., 2010). We previously demonstrated the capability of PAT to image the microvasculature of the iris (Hu et al., 2010; Rao et al., 2010). Other investigators evaluated OCT guided PAT (Jiao et al., 2010; Song et al., 2013) and laser-scanning optical-resolution PAT for retinal vasculature imaging and adaptive optics PAT to image single retinal pigment epithelium cells (Jiang et al., 2010; Xie et al., 2009). In the current study, we successfully imaged and resolved sO_2 in the ciliary body of the rabbit eye with AR PAT.

Our pilot study has limitations. Due to strong scleral scattering, we used AR PAT (Zhang et al., 2006) in the experiment. The lateral resolution of AR PAT is 80 microns, which is larger than the diameter of microvasculature, so it is not possible to resolve individual blood vessels with a diameter less than 80 microns. However, the system can integrate the optical-resolution capability to get deep vessel images of the ciliary body (Xing et al., 2013). Because the laser only has an 1 kHz repetition rate, there were strong motion artifacts, which reduced current measurement accuracy. In the future, a video-rate AR PAT system can be employed to increase the monitoring speed and thus decrease motion artifacts (Wang et al., 2012). And last but not least our study did not demonstrate the accuracy of AR PAT's sO_2 values. Future studies involving tissue phantoms would help to determine the accuracy of sO_2 values obtained with AR PAT.

Despite these limitations, our pilot study found that the AR PAT imaging modality is capable of obtaining non-invasively *in vivo* sO_2 qualitative monitoring correlated with pulse oximetry under various oxygen blood levels in rabbits. Further studies are needed to validate and modify the PAT modality specifically for ophthalmic use. Safe, non-invasive *in vivo* PAT imaging of the anterior segment and, potentially, the posterior segment of the eye, would be useful for evaluating the role of oxidative damage, hypoxia and ischemia in pathogenesis of various ocular diseases such as glaucoma, diabetic retinopathy, age-related macular degeneration and cataract.

Dedication

We dedicate this manuscript to David Beebe, PhD, who's recent passing from ALS deeply shocked and saddened all of us. David Beebe was an energetic, passionate, and insightful scientist and a wonderful mentor for many of us. He was someone who never

wasted a moment of his life. He was a sterling example of how compassion, motivation, and kindness can change the world. But most of all he was such a great person. People like David change the world because everyone tries to do a little more and do a little better because of his example. He will be greatly missed.

Sources of funding

This work is supported, in part, by a Faculty Diversity grant, Washington University in St. Louis, # 93711 (SNH) and by National Institutes of Health grants R01 EB008085, R01 CA134539, U54 CA136398, R01 CA159959, DP1 EB016986 (NIH Director's Pioneer Award) (LVW).

Conflicts of interest

Stella N. Hennen: none; Wenxin Xing: none; Ying-Bo Shui: none; Yong Zhou: none; Kalishman Jennifer: none; Andrews-Kaminsky, Lisa: none; Michael Kass: none; Beebe, David: none; Maslov, Konstantin: Microphotoacoustics, Inc., which, however, did not support this work; Wang, Lihong: Microphotoacoustics, Inc. and Endra, Inc., which, however, did not support this work.

References

- Abu-Amero, K.K., Morales, J., Bosley, T.M., 2006. Mitochondrial abnormalities in patients with primary open-angle glaucoma. *Invest. Ophthalmol. Vis. Sci.* 47, 2533–2541.
- Alvarado, J., Murphy, C., Polansky, J., Juster, R., 1981. Age-related changes in trabecular meshwork cellularity. *Invest. Ophthalmol. Vis. Sci.* 21, 714–727.
- Chang, S., 2006. LXII Edward Jackson lecture: open angle glaucoma after vitrectomy. *Am. J. Ophthalmol.* 141, 1033–1043.
- Chen, J.Z., Kadlubar, F.F., 2003. A new clue to glaucoma pathogenesis. *Am. J. Med.* 114, 697–698.
- Culver, J.P., Durduran, T., Furuya, T., Cheung, C., Greenberg, J.H., Yodanis, A.G., 2003. Diffuse optical tomography of cerebral blood flow, oxygenation, and metabolism in rat during focal ischemia. *J. Cereb. Blood Flow. Metab.* 23, 911–924.
- de la Zorda, A., Paulus, Y.M., Teed, R., Bodapati, S., Dollberg, Y., Khuri-Yakub, B.T., Blumenkranz, M.S., Moshfeghi, D.M., Gambhir, S.S., 2010. Photoacoustic ocular imaging. *Opt. Lett.* 35, 270–272.
- Ferreira, S.M., Lerner, S.F., Brunzini, R., Evelson, P.A., Llesuy, S.F., 2004. Oxidative stress markers in aqueous humor of glaucoma patients. *Am. J. Ophthalmol.* 137, 62–69.
- Gabelt, B.A.T., Kaufman, P.L., 2005. Changes in aqueous humor dynamics with age and glaucoma. *Prog. Retin. Eye Res.* 24, 612–637.
- Hoelen, C.G., de Mul, F.F., Pongers, R., Dekker, A., 1998. Three-dimensional photoacoustic imaging of blood vessels in tissue. *Opt. Lett.* 23, 648–650.
- Holekamp, N.M., Shui, Y.B., Beebe, D.C., 2005. Vitrectomy surgery increases oxygen exposure to the lens: a possible mechanism for nuclear cataract formation. *Am. J. Ophthalmol.* 139, 302–310.

- Hu, S., Rao, B., Maslov, K., Wang, L.V., 2010. Label-free photoacoustic ophthalmic angiography. *Opt. Lett.* 35, 1–3.
- Izzotti, A., Bagnis, A., Sacca, S.C., 2006. The role of oxidative stress in glaucoma. *Mutat. Res.* 612, 105–114.
- Izzotti, A., Sacca, S.C., Cartiglia, C., De Flora, S., 2003. Oxidative deoxyribonucleic acid damage in the eyes of glaucoma patients. *Am. J. Med.* 114, 638–646.
- Izzotti, A., Sacca, S.C., Longobardi, M., Cartiglia, C., 2009. Sensitivity of ocular anterior chamber tissues to oxidative damage and its relevance to the pathogenesis of glaucoma. *Invest. Ophthalmol. Vis. Sci.* 50, 5251–5258.
- Jiang, M., Zhang, X., Puliafito, C.A., Zhang, H.F., Jiao, S., 2010. Adaptive optics photoacoustic microscopy. *Opt. Express* 18, 21770–21776.
- Jiao, S., Jiang, M., Hu, J., Fawzi, A., Zhou, Q., Shung, K.K., Puliafito, C.A., Zhang, H.F., 2010. Photoacoustic ophthalmoscopy for in vivo retinal imaging. *Opt. Express* 18, 3967–3972.
- Jiao, S., Xie, Z., Zhang, H.F., Puliafito, C.A., 2009. Simultaneous multimodal imaging with integrated photoacoustic microscopy and optical coherence tomography. *Opt. Lett.* 34, 2961–2963.
- Kinnunen, K., Petrovski, G., Moe, M.C., Berta, A., Kaarniranta, K., 2012. Molecular mechanisms of retinal pigment epithelium damage and development of age-related macular degeneration. *Acta Ophthalmol.* 90, 299–309.
- Kong, F., Chen, Y.C., Lloyd, H.O., Silverman, R.H., Kim, H.H., Cannata, J.M., Shung, K.K., 2009a. High-resolution photoacoustic imaging with focused laser and ultrasonic beams. *Appl. Phys. Lett.* 94, 33902.
- Kong, G.Y., Van Bergen, N.J., Trounce, I.A., Crowston, J.G., 2009b. Mitochondrial dysfunction and glaucoma. *J. Glaucoma* 18, 93–100.
- Liang, J., Zhou, Y., Maslov, K.I., Wang, L.V., 2013. Cross-correlation-based transverse flow measurements using optical-resolution photoacoustic microscopy with a digital micromirror device. *J. Biomed. Opt.* 18 (9), 096004.
- Liton, P.B., Lin, Y., Gonzalez, P., Epstein, D.L., 2009. Potential role of lysosomal dysfunction in the pathogenesis of primary open angle glaucoma. *Autophagy* 5, 122–124.
- Maslov, K., Zhang, H.F., Hu, S., Wang, L.V., 2008. Optical-resolution photoacoustic microscopy for in vivo imaging of single capillaries. *Opt. Lett.* 33, 929–931.
- Rao, B., Li, L., Maslov, K., Wang, L., 2010. Hybrid-scanning optical-resolution photoacoustic microscopy for in vivo vasculature imaging. *Opt. Lett.* 35, 1521–1523.
- Rosenzweig, A., 1982. Potential clinical applications of photoacoustics. *Clin. Chem.* 28, 1878–1881.
- Sacca, S.C., Izzotti, A., Rossi, P., Traverso, C., 2007. Glaucomatous outflow pathway and oxidative stress. *Exp. Eye Res.* 84, 389–399.
- Sacca, S.C., Izzotti, A., 2008. Oxidative stress and glaucoma: injury in the anterior segment of the eye. *Prog. Brain Res.* 173, 385–407.
- Sacca, S.C., Pascotto, A., Camicione, P., Capris, P., Izzotti, A., 2005. Oxidative DNA damage in the human trabecular meshwork: clinical correlation in patients with primary open-angle glaucoma. *Arch. Ophthalmol.* 123, 458–463.
- Shui, Y.B., Fu, J.J., Garcia, C., Dattilo, L.K., Rajagopal, R., McMillan, S., Mak, G., Holekamp, N.M., Lewis, A., Beebe, D.C., 2006. Oxygen distribution in the rabbit eye and oxygen consumption by the lens. *Invest. Ophthalmol. Vis. Sci.* 47, 1571–1580.
- Siegfried, C.J., Shui, Y., Holekamp, N.M., Bai, F., Beebe, D.C., 2010. Oxygen distribution in the human eye: relevance to the etiology of open angle glaucoma after vitrectomy. *Invest. Ophthalmol. Vis. Sci.* 51, 5731–5738.
- Silverman, R.H., Kong, F., Chen, Y.C., Lloyd, H.O., Kim, H.H., Cannata, J.M., Shung, K.K., Coleman, D.J., 2010. High-resolution photoacoustic imaging of ocular tissues. *Ultrasound Med. Biol.* 36, 733–742.
- Song, W., Wei, Q., Jiao, S., Zhang, H.F., 2013. Integrated photoacoustic ophthalmoscopy and spectral-domain optical coherence tomography. *J. Vis. Exp.* 15, e4390.
- Tomarev, S.I., 2001. Eyeing a new route along an old pathway. *Nat. Med.* 7, 294–295.
- Varma, S.D., Kovtun, S., Hegde, K.R., 2011. Role of ultraviolet irradiation and oxidative stress in cataract formation—medical prevention by nutritional antioxidants and metabolic agonists. *Eye Contact Lens* 37, 233–245.
- Wang, L., Maslov, K., Xing, W., Garcia-Urbe, A., Wang, L.V., 2012. Video-rate functional photoacoustic microscopy at depths. *J. Biomed. Opt.* 17, 106007.
- Wang, L.V., Wu, H., 2007. *Biomedical Optics: Principles and Imaging*. Wiley & Sons, Hoboken, New Jersey.
- Wang, L.V., 2008. Prospects of photoacoustic tomography. *Med. Phys.* 35, 5758–5767.
- Wang, N., Chintala, S.K., Fini, M.E., Schuman, J.S., 2001. Activation of a tissue-specific stress response in the aqueous outflow pathway of the eye defines the glaucoma disease phenotype. *Nat. Med.* 7, 304–309.
- Wang, X., Pang, Y., Ku, G., Stoica, G., Wang, L.V., 2003. Three-dimensional laser-induced photoacoustic tomography of mouse brain with the skin and skull intact. *Opt. Lett.* 28, 1739–1741.
- Wang, X., Xie, X., Ku, G., Wang, L.V., Stoica, G., 2006. Noninvasive imaging of hemoglobin concentration and oxygenation in the rat brain using high-resolution photoacoustic tomography. *J. Biomed. Opt.* 11, 024015.
- Wang, Y., Hu, S., Maslov, K., Zhang, Y., Xia, Y., Wang, L.V., 2011. In vivo integrated photoacoustic and confocal microscopy of hemoglobin oxygen saturation and oxygen partial pressure. *Opt. Lett.* 36, 1029–1031.
- Xie, Z., Jiao, S., Zhang, H.F., Puliafito, C.A., 2009. Laser-scanning optical-resolution photoacoustic microscopy. *Opt. Lett.* 34, 1771–1773.
- Xing, W., Wang, L., Maslov, K., Wang, L.V., 2013. Integrated optical- and acoustic-resolution photoacoustic microscopy based on an optical fiber bundle. *Opt. Lett.* 38, 52–54.
- Yao, J., Wang, L.V., 2011. Photoacoustic tomography : fundamentals, advances and prospects. *Contrast Media Mol. Imaging* 6, 332–345.
- Yee, S.H., Lee, K., Jerabek, P.A., Fox, P.T., 2006. Quantitative measurement of oxygen metabolic rate in the rat brain using microPET imaging of briefly inhaled O-15-labelled oxygen gas. *Nucl. Med. Commun.* 27, 573–581.
- Zhang, H.F., Maslov, K., Sivaramakrishnan, M., Stoica, G., Wang, L.H.V., 2007. Imaging of hemoglobin oxygen saturation variations in single vessels in vivo using photoacoustic microscopy. *Appl. Phys. Lett.* 90, 053901–053903.
- Zhang, H.F., Maslov, K., Stoica, G., Wang, L.V., 2006. Functional photoacoustic microscopy for high-resolution and noninvasive in vivo imaging. *Nat. Biotechnol.* 24, 848–851.
- Zhang, H.F., Wang, J., Wei, Q., Liu, T., Jiao, S., Puliafito, C.A., 2010a. Collecting back-reflected photons in photoacoustic microscopy. *Opt. Express* 18, 1278–1282.
- Zhang, X., Jiang, M., Fawzi, A.A., Li, X., Shung, K.K., Puliafito, C.A., Zhang, H.F., Jiao, S., 2010b. Simultaneous dual molecular contrasts provided by the absorbed photons in photoacoustic microscopy. *Opt. Lett.* 35, 4018–4020.
- Zhou, L., Li, Y., Yue, B.Y., 1999. Oxidative stress affects cytoskeletal structure and cell-matrix interactions in cells from an ocular tissue: the trabecular meshwork. *J. Cell. Physiol.* 180, 182–189.
- Zhou, Y., Liang, J., Maslov, K.I., Wang, L.V., 2013. Calibration-free transverse blood flow measurement based on time-domain cross correlation using photoacoustic microscopy in vivo. *Opt. Lett.* 38, 3882–3885.